High-pressure phase of cold-compressed bulk graphite and graphene nanoplatelets

Ilias Efthimiopoulos [1,2,*] Elissaios Stavrou [3,4,5] Koichiro Umemoto,[6] Sathish Mayanna,[2,7] Antonius Torode,[1]
Jesse S. Smith,[8] Stella Chariton [9] Vitali B. Prakapenka,[9] Alexander F. Goncharov,[10] and Yuejian Wang [1,†]

[1]*Department of Physics, Oakland University, Rochester, Michigan 48309, USA*

[2]*GFZ German Research Center for Geosciences, Telegrafenberg, 14473 Potsdam, Germany*

[3]*Materials Science and Engineering Program, Guangdong Technion–Israel Institute of Technology, Shantou, Guangdong 515063, China*

[4]*Department of Materials Science and Engineering, Technion–Israel Institute of Technology, Haifa 32000, Israel*

[5]*Guangdong Provincial Key Laboratory of Materials and Technologies for Energy Conversion, Guangdong Technion–Israel Institute
of Technology, Shantou, Guangdong 515063, China*

[6]*Earth-Life Science Institute, Tokyo Institute of Technology, Meguro, Tokyo 150–8550, Japan*

[7]*Carl Zeiss Microscopy GmbH, Carl Zeiss Strasse 22, 73447 Oberkochen, Germany*

[8]*HPCAT, X-ray Science Division, Argonne National Laboratory, Argonne, Illinois 60439, USA*

[9]*Center for Advanced Radiation Sources, University of Chicago, Chicago, Illinois 60637, USA*

[10]*Earth and Planets Laboratory, Carnegie Institution of Washington, Washington, DC 20015, USA*

We have studied the high-pressure vibrational and structural behavior of bulk graphite and graphene nanoplatelets at room temperature by means of high-pressure Raman spectroscopic and x-ray diffraction probes. We have detected a clear pressure-induced structural transition in both materials, evidenced by the appearance of new Bragg peaks and Raman features, deviating from the starting hexagonal graphitic structure. The high-pressure phase is identified as a partially disordered orthorhombic structure, consisting of mixed sp^2- and sp^3-type bonding. Our experimental findings serve as direct evidence for the existence of a metastable transient modification in cold compressed carbon, lying between the sp^2-type graphite and sp^3-type diamond allotropes.

I. INTRODUCTION

The versatility of elemental carbon to form structures made up of sp-, sp^2-, and sp^3-type bonding results in a rich variety of allotropes, both in the bulk, as well as in the nanoscale [1–4]. The stable three-dimensional phase of carbon at ambient conditions is the hexagonal graphite phase (HG), made up of planar sheets of six-membered sp^2-bonded carbon rings with AB-type (Bernal) stacking along the hexagonal *c* axis. Application of joint pressure and temperature transforms this phase into the sp^3-bearing diamond polymorphs, with profound industrial applications [5–7].

At room temperature, compression of bulk graphite leads to a new modification with increased electrical resistivity [8], optical transparency [9,10], and high hardness [3,11–13]. These characteristics indicated that the high-pressure phase contains sp^3-type carbon bonding, similar to cubic diamond (CD). Several candidates emerged from the theoretical side as a means of identifying this high-pressure modification [14–17], with a monoclinic phase (dubbed M-carbon) proposed to show the best agreement with the available ex-

perimental results [18]. It should be pointed out, however, that specific experimental observations, such as the absence of a clear sp^3-derived Raman signal [19–22], as well as the reversibility of the starting HG phase upon decompression [13,20–22], appear to contradict the general consensus of a purely sp^3-bearing high-pressure carbon phase under cold compression [4,13–16,18,23–28]. Thus, the high-pressure structure of cold compressed graphite still remains an open question.

Similar to the bulk graphite studies, recent investigations on graphene samples of varying layer numbers indicate the direct transformation of the starting HG to a semiconducting phase under compression [29–33]. This high-pressure graphene modification was inferred to adopt a hexagonal diamondlike (HD) structure [29–31]. The pressure-induced HG → HD formation at room temperature has been reported for bulk graphite as well [13], but was eventually dismissed [12,18]. The HD (lonsdaleite) represents a metastable carbon modification, acting as an "intermediate" phase between HG and CD [1,3]. The existence of HD as a discrete material, however, has been debated in recent literature [34,35]. For the sake of completeness, we should also mention that compression of glassy carbon at room temperature has been proposed to yield disordered diamondlike modifications [34,36–39]; this suggestion, however, has been also questioned [40,41].

In order to explore this matter further, we examined the high-pressure vibrational and structural behavior of both bulk

---

*Corresponding author: i.efthimiopoulos@mpie.de; Present address: Max-Planck-Institut für Eisenforschung GmbH, Max-Planck-Strasse 1, 40237 Düsseldorf, Germany.

†Corresponding author: ywang235@oakland.edu

natural graphite (NG) and graphene nanoplatelets (GNPs) at room temperature. The reason for choosing GNPs for our studies comes from the fact that the latter represent a "hybrid" system, structurally lying between bulk graphite and graphene [42]. Regarding GNPs, a recent high-pressure Raman spectroscopic study indicated a transition from the starting sp^2- to an sp^3-bearing phase close to 15 GPa [43]; no structural data were reported, however, to support this claim. Here we have probed the high-pressure structural and vibrational behavior of both bulk graphite and GNPs under cold compression. Our results indicate the formation of a metastable *partially disordered* orthorhombic modification, consisting of mixed sp^2- and sp^3-type carbon bonding. The existence of such a hybrid transient, made up of mixed sp^2- and sp^3-type bonding motif, promotes the understanding of the transformation mechanism in cold compressed graphite.

II. EXPERIMENTAL AND COMPUTATIONAL DETAILS

The NG single-crystalline sample is the same as in Refs. [21,44,45]. We should note here that there is a recorded dependence of the high-pressure behavior of bulk graphite on the sample quality. In particular, a deviating pressure-induced evolution in the optical and vibrational properties between natural, pyrolytic, and amorphous bulk graphite has been demonstrated, attributed to the higher percentage of stacking disorder present in the latter two samples [44]. In order to bypass this issue, we have investigated a high-quality and well-characterized NG sample. On the other hand, the graphene nanoplatetets exhibited an average thickness around 4 nm (i.e., ~12 graphene layers), and were purchased commercially (Grade 4, Purity >99 wt%); detailed characterization of the GNPs probed in this work can be found in Ref. [46].

Pressure was generated with diamond anvil cells (DACs), equipped with 300 and 400 μm culet diamonds. The angle-resolved high-pressure x-ray diffraction (XRD) measurements were performed at the GeoSoilEnviroCARS (Sector 13) and at the High-Pressure Collaborative Access Team (HPCAT, Sector 16), Advanced Photon Source, Argonne National Laboratory, with the newly commissioned multi-channel collimator. Helium (NG) and neon (GNPs) served as pressure transmitting media (PTM). The XRD patterns were processed with the DIOPTAS software [47]. Le Bail refinements were performed with the GSAS+EXPGUI software packages [48]. The ruby luminescence method was used for measuring pressure [49]. The Ne (PTM) equation of state [50,51] served as am additional pressure calibrant in the GNPs XRD run.

High-pressure Raman investigations were conducted with Ar$^+$ ($\lambda = 457$ nm, NG) and solid-state lasers ($\lambda = 532$ nm, GNPs) coupled to single-stage Raman spectrometers operating with a 1800 g/mm diffraction grating and charged-coupled device detectors. Neon (NG) and helium (GNPs) served as PTM in separate experimental runs.

The structural and vibrational properties of the HG and the rhombohedral graphite (RG) phases were calculated within the local-density approximation (LDA) [52,53]. The carbon pseudopotential was generated using Vanderbilt's method [54]. Cutoff radii for $2s$, $2p$, and $3d$ states are 1.3 a.u. The plane-wave cutoff energy is 50 Ry. We used variable-cell-shape molecular dynamics [55,56] for structural optimization under arbitrary pressure. The vibrational spectrum was obtained using density functional perturbation theory [57,58]. Further details on the computations can be found in Ref. [15].

III. RESULTS AND DISCUSSION

A. Structural properties of NG and GNPs under pressure

The XRD patterns of GNPs are shown collectively in Fig. 1(a). Under compression, new features arise close to 22 GPa. These new Bragg peaks are not compatible anymore with the starting HG phase, thus signaling the onset of a pressure-induced structural transformation in GNPs. The new modification dominates the XRD patterns at 34 GPa, where the structural transformation is completed. In the case of NG on the other hand, the HG phase is being "replaced" by a new structure at 25 GPa already [Fig. 1(b)]. The structural transition pressures are compatible with previous investigations on both bulk graphite and multi/few-layered graphene samples, with the latter exhibiting generally higher transition pressure values (inversely proportional to the number of layers) [9,13,18,21,29,32].

Admittingly, in the bulk NG XRD patterns, the structural transition from the starting HG to the high-pressure modfication is less discernible compared to the GNPs case (Fig. 1). Plotting of the Bragg peak pressure dependence for both NG and GNPs, however, resolves this issue. In Fig. 2(a) we can clearly assign the specific HG and high-pressure phase XRD features by following the respective pressure-induced evolution, and conclude that the latter is the dominant phase for both samples above 35 GPa [Fig. 2(a)]. Consequently, in Fig. 2(b) we show the XRD patterns of both NG and GNPs at the highest pressure achieved in each experimental run, namely at 38 GPa and 37.4 GPa. Both XRD patterns show virtually identical Bragg features, indicating that both GNPs and NG adopt the same high-pressure phase. We tried several of the theoretically predicted sp^3-bearing modifications [14–17], including the CD, HD, and M-carbon phases. None of the proposed structures, however, provided satisfactory agreement with the experimental XRD patterns [59].

By setting particular volume constraints, i.e., by restricting the volume per atom of the high-pressure phase between the extrapolated HG (upper limit) and the CD (lower limit) volume values (Fig. 3), our XRD patterns are best indexed to an orthorhombic unit cell with lattice parameters: $a = 2.424$ Å, $b = 3.803$ Å, $c = 5.449$ Å, $V = 50.23$ Å^3 at ~38 GPa [NG, Fig. 2(b)]. We term this phase as high-pressure orthorhombic graphite (HP-OG) from this point onward. Interestingly, our evaluated lattice parameters fall in line with the orthorhombic graphite (quinoid) structure proposed by Pauling for bulk graphite at ambient conditions decades ago, a structure which allows for a much more efficient layer stacking [61]. It must be pointed out, however, that the measured Bragg peaks belonging to the high-pressure phase are quite broad (width ≈0.1 Å^{-1}) and asymmetric, hinting *sizeable structural disorder* and/or formation of nanodomains present in HP-OG [59]. This is the main reason for the relatively unsatisfying quality of our Le Bail refinements [Fig. 2(b)]. Consequently, a unique space group cannot be provided at this stage.
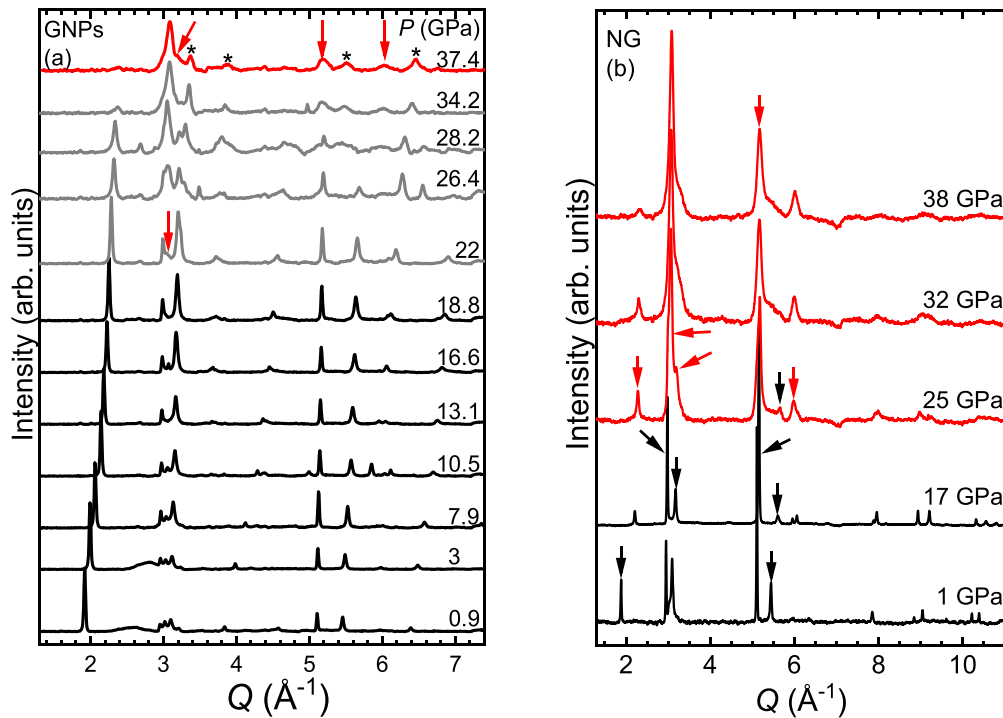
FIG. 1. (a) Normalized XRD patterns of GNPs ($\lambda = 0.3344$ Å, $T = 300$ K, $Q = \lambda^{-1} 4\pi \sin\theta$, Ne as PTM) and (b) the bulk NG sample ($\lambda = 0.2952$ Å, $T = 300$ K, $Q = \lambda^{-1} 4\pi \sin\theta$, He as PTM) at various pressures. The black, red, and grey colors correspond to the HG and HP-OG phases, and the coexistence regime, respectively. Background has been subtracted for clarity. The black and red arrows denote the Bragg peaks assigned exclusively to the HG and the HP-OG phase, respectively. Asterisks indicate Ne PTM peaks. Notice that the use of He as PTM does not contaminate our XRD patterns with additional Bragg peaks, thus allowing for the detection of the NG Bragg peaks alone.

The volume reduction at the HG → HP-OG transition point is estimated at ∼8%, significantly less than the expected volume change for a complete $sp^2 \rightarrow sp^3$-type transition (Fig. 3). On the other hand, the measured HP-OG XRD patterns resemble strongly that of cubic diamond, thus hinting a close structural connection between the two phases [Figs. 2(b) and S3] [59]. From this similarity alone, one may hypothesize that the HP-OG phase must contain sp^3-bonded carbon. The presence of sp^3-type carbon can be further advocated by the calculated HP-OG bulk modulus value (525 ± 20 at 25 GPa), which lies in the superhard regime (Table I). Hence, the question is: *What is the nature of this HP-OG phase, and how does it fit into the HG → Diamond transformation pathway*?

B. Raman spectroscopic studies under compression

Additional insights on the transformation mechanism of the HG phase under cold compression is gained from our Raman spectroscopic investigations. In Fig. 4 we present selected Raman spectra for the bulk NG sample at various pressures, below and above the diamond (DAC) Raman peak. Initially we observe only the HG G-band at ∼1650 cm^{-1} up to 15 GPa. Upon increasing pressure at 20 GPa, three new modes are appearing in our Raman spectra: one low-frequency band at ∼90 cm^{-1}, a second Raman feature close to 860 cm^{-1}, and a broad and weak hump developing between the DAC diamond Raman peak and the G band at about 1450 cm^{-1}. Further compression enhances all of these new Raman features intensity wise (except the 90 cm^{-1} mode, which

gradually diminishes above 35 GPa), with the pressure rates being distinctly different: the 90 and 1450 cm^{-1} modes display an upshift with increasing pressure, whereas the 860 cm^{-1} band exhibits a modest *negative* pressure dependence up to 53 GPa (Fig. 5 and Table II). Taken together, these Raman-related changes indicate a phase transition in the NG sample initiating close to 20 GPa, consistent with our XRD investigations (Figs. 2 and 3). Each of these Raman features is discussed separately.

The 90 cm^{-1} mode is relatively sharp and displays an interesting behavior intensity-wise under pressure. In particular, its intensity increases in the 20 GPa $\leqslant P \leqslant$ 30 GPa pressure range, with further compression leading to its gradual diminishing. Actually, the pressure-induced intensity behavior of this band up to 30 GPa is analogous to that of the rigid layer HG-E_{2g} mode of graphite (Figs. 4 and S4) [59], where such an effect was attributed to electronic resonance and/or enhancement of the respective Raman cross section [22]. Our experimental data on a separate run of the NG sample (Fig. S4) [59], as well as our calculations (Fig. 5), hint that this 90 cm^{-1} band is a "descendant" of the HG−E_{2g} rigid-layer graphitic mode, persisting also in the HP-OG phase.

On the other hand, the soft-mode behavior of the 860 cm^{-1} band under pressure directly implies the structural/dynamic instability of the HP-OG phase, whereas it also excludes any of the predicted high-pressure phases composed solely from sp^3-type carbon bonding [64]. On the contrary, RG, a "faulted" version of HG with different stacking order, is predicted to exhibit a soft A_{1g} mode at about these frequencies
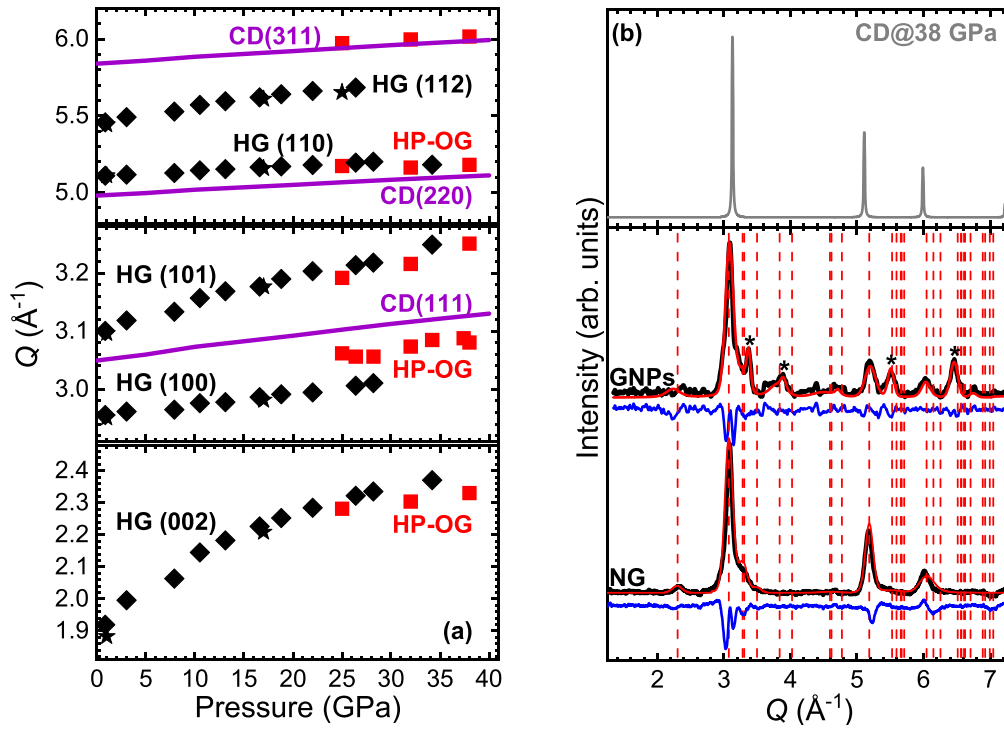
FIG. 2. (a) Pressure dependence of the HG Bragg peaks for the NG (black stars) and the GNPs (black diamonds). The adjacent Bragg peaks of the HP-OG phase are also plotted (red squares). The violet lines represent the Bragg peaks of cubic diamond (CD) [60]. The respective Miller indices are also provided for convenience. (b) Le Bail refinements of the XRD patterns of bulk natural graphite (NG, $\lambda = 0.2952$ Å, He PTM) and GNPs ($\lambda = 0.3344$ Å, Ne PTM) collected at 37–38 GPa. The black symbols stand for the experimental XRD pattern, the red and blue lines depicting the best refinement and difference curves, respectively. Vertical ticks mark the HP-OG Bragg peak positions. Asterisks stand for the Ne PTM peaks. The simulated XRD pattern of cubic diamond (CD) at 38 GPa is also drawn (top) [60].

[65]. Indeed, our DFT-LDA calculations on the RG phase reproduce and expand the A_{1g} mode softening over an extensive pressure range (Fig. 5). This RG A_{1g} vibration, which descends from the Raman-forbidden ZO phonon of HG [66], corresponds to carbon motions perpendicular to the graphitic

layers. The similar soft-mode behavior between the RG A_{1g} and HP-OG 860 cm^{-1} Raman features points to a common origin, i.e., out-of-plane carbon motions.

Turning next to the 1450 cm^{-1} Raman mode, this feature was taken as the signature of sp^3-type bonding in carbon nanohorns [67]. Even though the association of this feature
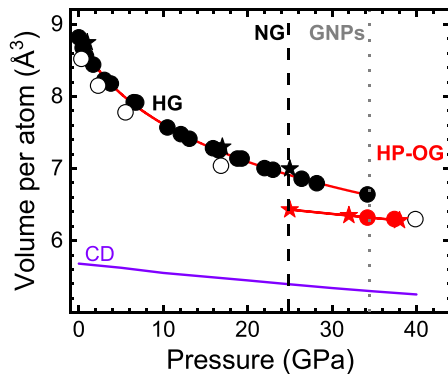

FIG. 3. Equations of state for the starting hexagonal graphite (HG, black) and the high-pressure (HP-OG, red) phases of GNPs and NG samples. The red solid lines passing through the *P-V* data (circles: GNPs, stars: NG) correspond to Birch-Murnaghan equation of state fittings [62,63], with the respective parameters tabulated in Table I. Open circles correspond to our LDA-calculated HG data [59]. The EOS of cubic diamond (CD, purple solid line) is also drawn [60].

TABLE I. Reduced volume V_0/Z, bulk modulus B_0, and its pressure derivative B_0' for various bulk graphite and GNPs' modifications, evaluated at ambient pressure. The data from this work are obtained by Birch-Murnaghan equation of state fittings [62,63] to the measured *P-V* data (Fig. 3) [59]. Selected data from literature are also provided for comparison.

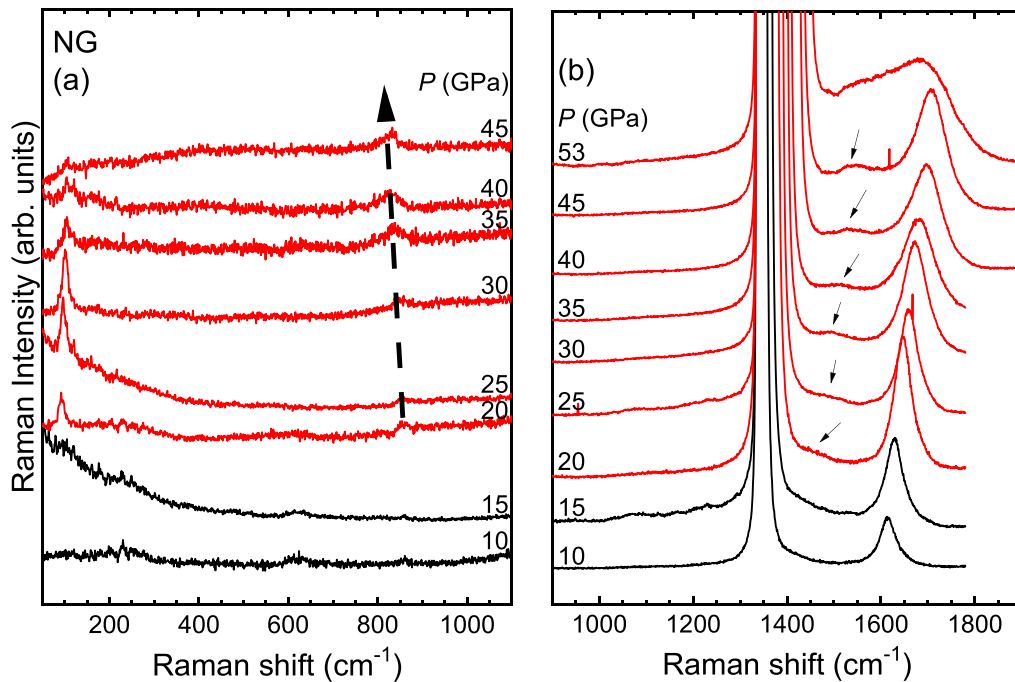| SG	Sample	V_0/Z(Å^3)	B_0 (GPa)	B_0'
$P6_3/mmc$	NG, GNPs	8.82(exp.)	35(2)	10.1(6)
	HG (DFT-LDA)	8.50	40	8.7
	HG [18]	8.82(1)	57.3(8)	4(fixed)
	HG [22]	8.78(2)	33.8(3)	8.9(1)
HP-OG	NG, GNPs[a]	6.43(exp.)	525(20)	4(fixed)
	M-carbon [16]	5.78	431.2	3.60
	Diamond [60]	5.67	446	5.47
	bct-C$_4$ [15]	5.82	428.7	2.56
	W-carbon [14]	5.76	444.5	4.39
	Z-carbon [17]	5.76	441.5	N/A

[a]EOS parameters evaluated at 25 GPa (Fig. 3).

FIG. 4. As-measured Raman spectra of the bulk NG graphite sample at selected pressures, with Ne serving as PTM ($\lambda = 457$ nm, $T = 300$ K). The spectra are divided between the (a) low-frequency and (b) high-frequency (G-band) regions. The black and red color corresponds to the HG and HP-OG phases, respectively.

with the presence of sp^3-type carbon is certainly appealing, specific literature results on carbon samples should be considered. Namely, the F-band of glassy carbon shows a virtually identical behavior with that of the 1450 cm^{-1} NG Raman feature (Fig. 5) [21,40]. Actually, the 53 GPa NG Raman spectrum shown here strongly resembles that of

glassy/amorphous carbon at this pressure, indicating some degree of structural disorder in the NG sample at these pressures [21,40,44]. Such disorder is consistent with the relatively broad Bragg peaks detected in our XRD studies, belonging to the high-pressure phase (Fig. 1).

C. The carbon phase diagram

Summarizing our XRD and Raman studies, we can reach the following conclusions: (1) Both the bulk NG and the GNPs adopt the same high-pressure phase at ambient temperature; (2) the XRD profile of the high-pressure phase is best reproduced using an orthorhombic unit cell (HP-OG); (3) the XRD and Raman features of the high-pressure phase are significantly broader with respect to their HG counterparts, hinting that the HP-OG modification incorporates some degree of structural disorder and/or nanodomain formation, supporting earlier Raman investigations on bulk and thin carbon film samples [21,68]; an additional piece of evidence in favor of the presence of disorder in the high-pressure carbon phase is the close affinity between the HP-OG and glassy/amorphous carbon Raman spectra; (4) the clear detection of a mode linked to the rigid-layer HG-E_{2g} Raman mode up to 40 GPa, the persistence of the G-band, the moderate volume drop at the HG → HP-OG transition, as well as the reversibility of the transition upon decompression (Fig. S6) [59] imply that the carbon bonding in the HP-OG phase retains substantial sp^2-type character; (5) considering on the other hand the measurable volume drop at the HG → HP-OG transition, the incompressibility of the HP-OG phase, the close resemblance of the HP-OG XRD profile with that of cubic diamond, as well as the optical band gap opening [9,20,45], resistivity increase
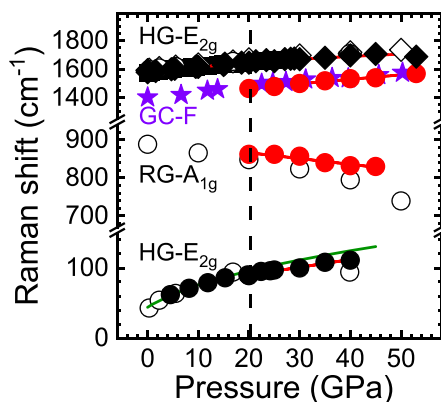

FIG. 5. Pressure-induced behavior of the Raman mode frequencies for bulk NG and GNPs (solid symbols). The black and red colors stand for the specific HG and HP-OG Raman-related feautures, respectively. The estimated HG-E_{2g} mode (green line) [22], the F-band of glassy carbon (GC-F, violet stars) [40] and our LDA-calculated HG and rhombohedral graphite (RG) mode frequencies (open symbols) are included for comparison. Solid lines passing through the experimental data represent least-square fittings (Table II). The vertical dashed line marks the onset pressure of the HG → HP-OG transition in the NG sample.

TABLE II. Mode frequency, pressure coefficients, and the mode Grüneisen parameter γ_i for the Raman bands of GNPs and bulk graphite. The Raman features are fitted with the polynomial function: $\omega(P) = \omega_0 + (\partial\omega/\partial P)*P + (\partial^2\omega/\partial P^2)*P^2$, where frequeny ω_0 is in cm^{-1} and pressure P in GPa. The mode Grüneisen parameter γ_i is determined from the relation: $\gamma_i = (B_0/\omega_0)\mathrm{x}(\partial\omega/\partial P)$, where $B_0 = 35$ GPa for GNPs and $B_0 = 33.8$ GPa for HG (Table I). The HP-OG data are calculated at 25 GPa, so as to use the $B_0 = 525$ GPa value (Table I).

Carbon form	PTM	Mode Symmetry	ω_0 (cm^{-1})	$\partial\omega/\partial P$ (cm^{-1}/GPa)	$\partial^2\omega/\partial P^2$ (cm^{-1}/GPa^2)	γ_i
GNPs	He	E_{2g}	1577.5	4.02	-0.03	0.09
GNPs	Ar	E_{2g}	1577.5	4.49	-0.04	0.10
Graphite-NG	Ne	E_{2g}	53.6	2.3(2)	-0.02	1.45
Graphite-NG	Ne	E_{2g}	1582.7	3.6(2)	-0.02	0.08
Graphite [22]	M/E 4:1	E_{2g}	44(1)	4.8	-	-
Graphite [22]	M/E 4:1	E_{2g}	1579(1)	4.7	-	0.10
Graphite-LDA (HG)	N/A	E_{2g}	1582	3.6(2)	-0.02	0.09
Graphite-LDA (RG)	N/A	B_{1g}	887	$-1.74(2)$	-	-0.08
HP-OG	Ne	N/A	98.6	2.3(2)	-0.02	12.25
HP-OG	Ne	N/A	859.3	$-1.5(2)$	-	-0.92
HP-OG	Ne	N/A	1482.4	3.2(2)	-	1.13
HP-OG	Ne	N/A	1660.5	1.48(6)	-	0.47

[8,69], and change of interplanar carbon bonding character in the high-pressure phase [12], one must acknowledge the existence of (at least partial) sp^3-type bonding in HP-OG, thus designating HP-OG as a *metastable sp^2/sp^3-bearing hybrid modification*. Taken together, the aforementioned characteristics make HP-OG comparable to glassy carbon from a structural viewpoint, made up also of hybrid sp^2/sp^3-type carbon bonding [38,41,70,71].

How does this metastable cold-compressed HP-OG hybrid fit into the carbon phase diagram [1,3] and what are the implications? In order to answer this question, we need to place our results into perspective with the available literature on the graphite → diamond transformation pathway, i.e., the transition from a fully sp^2-type to a fully sp^3-type carbon polymorph. Numerous modeling works on the HG → diamond transition have shown that the latter proceeds via an *intermediate* phase, which can be either a RG or an OG transient [25,72–77]. This "bridging" structure, which differs from HG with respect to the graphene layer stacking sequence [78], appears as a necessary precursor step prior to the adoption of either the CD or the HD diamond polytypes.

In contrast with the RG phase, which has been found to coexist with HG in natural and deformed graphite samples [79,80], the OG phase has not been reported experimentally. Instead, the available XRD patterns on bulk graphite and few-layered graphene samples have been assigned either to M-carbon [18] or HD-type [13,29] structures. In these works, however, the XRD diffractograms composed of one or two Bragg features specific to the high-pressure phase. Having at our disposal at least four clear Bragg features belonging exclusively to the high-pressure NG and GNPs phase, and considering the necessary volume constraints (Fig. 3), deems us confident regarding the assignment of an *average* orthorhombic symmetry to the high-pressure modification. Consequently, it is quite tempting to relate our HP-OG to the predicted OG transient, as the two share many common features.

The dynamic instability of HP-OG, indicated by the presence of a soft Raman-active mode (Figs. 4 and 5, Table II), directly indicates that HP-OG is on the verge of subsequent structural transformation(s) upon further compression and/or temperature treatment, in order to overcome potential energy/kinetic barriers. Actually, the apparent assignment of this soft-mode to out-of-plane carbon motions alludes also to the plausible deformation mechanism of HP-OG, involving mainly interplanar connectivity (e.g., sliding and/or buckling of carbon sheets). Such a mechanism would fall in line with HP-OG acting as a metastable/intermediate sp^2/sp^3−bearing transient state lying between the HG and diamond structures [72–75], advocating the possibility that HP-OG might indeed be the hypothetical OG modification, i.e., the structural link between the sp^2- and sp^3-type carbon polymorphs.

IV. CONCLUSIONS

We have investigated the high-pressure behavior of bulk natural graphite and GNPs at room temperature by means of high-pressure XRD and Raman spectroscopic probes. In both cases, we were able to detect the same pressure-induced structural transition. The measured data are consistent with a metastable modification with an *average* orthorhombic symmetry, encompassing nevertheless some degree of (local) structural disorder. We have termed this modification as high-pressure orthorhombic graphite (HP-OG). Both our XRD and Raman investigations indicate that HP-OG is composed of a sp^2/sp^3-type carbon bonding mixture, thus lying in-between the sp^2-bearing HG and the sp^3-type diamond phases. Such an intermediate carbon configuration with orthorhombic symmetry has been already considered from a theoretical perspective as a necessary precursor for the formation of diamond from graphite. This coincidence alludes a strong possibility that our metastable HP-OG phase is actually this predicted "bridging" state, linking structurally the sp^2- and sp^3-type carbon polymorphs.

[1] F. P. Bundy, W. A. Bassett, M. S. Weathers, R. J. Hemley, H.-K. Mao, and A. F. Goncharov, The pressure-temperature phase and transformation diagram for carbon; updated through 1994, Carbon N. Y. **34**, 141 (1996).

[2] V. Georgakilas, J. A. Perman, J. Tucek, and R. Zboril, Broad family of carbon nanoallotropes: Classification, chemistry, and applications of fullerenes, carbon dots, nanotubes, graphene, nanodiamonds, and combined superstructures, Chem. Rev. **115**, 4744 (2015).

[3] B. Sundqvist, Carbon under pressure, Phys. Rep. **909**, 1 (2021).

[4] Y. Wang and K. K. M. Lee, From soft to superhard: Fifty years of experiments on cold-compressed graphite, J. Superhard Mater. **34**, 360 (2012).

[5] P. W. May, Diamond thin films: A 21st-century material, Philos. Trans. R. Soc. A **358**, 473 (2000).

[6] J. A. Carlisle, Diamond films: Precious biosensors, Nat. Mater. **3**, 668 (2004).

[7] E. Stavrou, M. Bagge-Hansen, J. A. Hammons, M. H. Nielsen, B. A. Steele, P. Xiao, M. P. Kroonblawd, M. D. Nelms, W. L. Shaw, W. Bassett, S. Bastea, L. M. Lauderbach, R. L. Hodgin, N. A. Perez-Marty, S. Singh, P. Das, Y. Li, A. Schuman, N. Sinclair, K. Fezzaa, A. Deriy, L. D. Leininger, and T. M. Willey, Detonation-induced transformation of graphite to hexagonal diamond, Phys. Rev. B **102**, 104116 (2020).

[8] R. B. Aust and H. G. Drickamer, Carbon: A new crystalline phase, Science **140**, 817 (1963).

[9] W. Utsumi and T. Yagi, Light-transparent phase formed by room-temperature compression of graphite, Science **252**, 1542 (1991).

[10] M. Hanfland, K. Syassen, and R. Sonnenschein, Optical reflectivity of graphite under pressure, Phys. Rev. B **40**, 1951 (1989).

[11] F. P. Bundy and J. S. Kasper, Hexagonal diamond—a new form of carbon, J. Chem. Phys. **46**, 3437 (1967).

[12] W. L. Mao, H.-K. Mao, P. J. Eng, T. P. Trainor, M. Newville, C.-C. Kao, D. L. Heinz, J. Shu, Y. Meng, and R. J. Hemley, Bonding changes in compressed superhard graphite, Science **302**, 425 (2003).

[13] T. Yagi, W. Utsumi, M. A. Yamakata, T. Kikegawa, and O. Shimomura, High-pressure *in situ* x-ray diffraction study of the phase transformation from graphite to hexagonal diamond at room temperature, Phys. Rev. B **46**, 6031 (1992).

[14] J. T. Wang, C. Chen, and Y. Kawazoe, Low-Temperature Phase Transformation from Graphite to Sp^3 Orthorhombic Carbon, Phys. Rev. Lett. **106**, 075501 (2011).

[15] K. Umemoto, R. M. Wentzcovitch, S. Saito, and T. Miyake, Body-Centered Tetragonal C4: A Viable Sp^3 Carbon Allotrope, Phys. Rev. Lett. **104**, 125504 (2010).

[16] Q. Li, Y. Ma, A. R. Oganov, H. Wang, H. Wang, Y. Xu, T. Cui, H.-K. Mao, and G. Zou, Superhard Monoclinic Polymorph of Carbon, Phys. Rev. Lett. **102**, 175506 (2009).

[17] M. Amsler, J. A. Flores-Livas, L. Lehtovaara, F. Balima, S. A. Ghasemi, D. Machon, S. Pailhes, A. Willand, D. Caliste, S. Botti, A. SanMiguel, S. Goedecker, and M. A. L. Marques, Crystal Structure of Cold Compressed Graphite, Phys. Rev. Lett. **108**, 065501 (2012).

[18] Y. Wang, J. E. Panzik, B. Kiefer, and K. K. M. Lee, Crystal structure of graphite under room-temperature compression and decompression, Sci. Rep. **2**, 520 (2012).

[19] J. Xu, H.-K. Mao, and R. J. Hemley, The gem anvil cell: High-pressure behaviour of diamond and related materials, J. Phys. Condens. Matter. **14**, 11549 (2002).

[20] E. D. Miller, D. C. Nesting, and J. V. Badding, Quenchable transparent phase of carbon, Chem. Mater. **9**, 18 (1997).

[21] A. F. Goncharov, Graphite at high pressures: Amorphization at 44 GPa, High Press. Res. **8**, 607 (1992).

[22] M. Hanfland, H. Beister, and K. Syassen, Graphite under pressure: Equation of state and first-order raman modes, Phys. Rev. B **39**, 12598 (1989).

[23] X.-F. Zhou, G.-R. Qian, X. Dong, L. Zhang, Y. Tian, and H.-T. Wang, *Ab Initio* study of the formation of transparent carbon under pressure, Phys. Rev. B **82**, 134126 (2010).

[24] S.-C. Zhu and Q.-Y. Hu, Unraveling the structural transition mechanism of room-temperature compressed graphite carbon, Phys. Chem. Chem. Phys. **23**, 20560 (2021).

[25] S. E. Boulfelfel, A. R. Oganov, and S. Leoni, Understanding the nature of superhard graphite, Sci. Rep. **2**, 471 (2012).

[26] C. He, L. Sunn, C. Zhang, X. Peng, K. Zhang, and J. Zhong, New superhard carbon phases between graphite and diamond, Solid. State. Commun. **152**, 1560 (2012).

[27] X. Yuan, Y. Cheng, H. Tang, P. Wang, F. Liu, S. Han, J. Zhu, M.-S. Wang, and L. Wang, Sp^2-to-Sp^3 transitions in graphite during cold-compression, Phys. Chem. Chem. Phys. **24**, 10561 (2022).

[28] R. Zhou and X. C. Zheng, Polymorphic phases of Sp^3-hybridized carbon under cold compression, J. Am. Chem. Soc. **134**, 7530 (2012).

[29] F. Ke, L. Zhang, Y. Chen, K. Yin, C. Wang, Y.-K. Tzeng, Y. Lin, H. Dong, Z. Liu, J. S. Tse, W. L. Mao, J. Wu, and B.

Chen, Synthesis of atomically thin hexagonal diamond with compression, Nano Lett. **20**, 5916 (2020).

[30] L. G. P. Martins, M. J. S. Matos, A. R. Paschoal, P. T. C. Freire, N. F. Andrade, A. L. Aguiar, J. Kong, B. R. A. Neves, A. B. de Oliveira, M. S. C. Mazzoni, A. G. S. Filho, and L. G. Cancado, Raman evidence for pressure-induced formation of diamondene, Nat. Commun. **8**, 96 (2017).

[31] A. P. M. Barboza, M. H. D. Guimaraes, D. V. P. Massote, L. C. Campos, N. M. B. Neto, L. G. Cancado, R. G. Lacerda, H. Chacham, M. S. C. Mazzoni, and B. R. A. Neves, Room-temperature compression-induced diamondization of few-layer graphene, Adv. Mater. **23**, 3014 (2011).

[32] F. Ke, Y. Chen, K. Yin, J. Yan, H. Zhang, Z. Liu, J. S. Tse, J. Wu, H.-K. Mao, and B. Chen, Large bandgap of pressurized trilayer graphene, Proc. Natl Acad. Sci. **116**, 9186 (2019).

[33] L. G. P. Martins, D. L. Silva, J. S. Smith, A.-Y. Lu, C. Su, M. Hempel, C. Occhialini, X. Ji, R. Pablo, R. S. Alencar, A. C. R. Souza, A. A. Pinto, A. B. de Oliveira, R. J. C. Batista, T. Palacios, M. S. C. Mazzoni, M. J. S. Matos, R. Comin, J. Kong, and L. G. Cancado, Hard, transparent, Sp^3-containing 2D phase formed from few-layer graphene under compression, Carbon N. Y. **173**, 744 (2021).

[34] T. B. Shiell, D. G. McCulloch, J. E. Bradby, B. Haberl, R. Boehler, and D. R. McKenzie, Nanocrystalline hexagonal diamond formed from glassy carbon, Sci. Rep. **6**, 37232 (2016).

[35] P. Nemeth, L. A. J. Garvie, T. Aoki, N. Dubrovinskaia, L. Dubrovinsky, and P. R. Buseck, Lonsdaleite is faulted and twinned cubic diamond and does not exist as a discrete material, Nat. Commun. **5**, 5447 (2014).

[36] D. G. McCulloch, S. Wong, T. B. Shiell, B. Haberl, B. A. Cook, X. Huang, R. Boehler, D. R. McKenzie, and J. E. Bradby, Investigation of room temperature formation of the ultra-hard nanocarbons diamond and lonsdaleite, Small **16**, 2004695 (2020).

[37] Z. Zeng, L. Yang, Q. Zeng, H. Lou, H. Sheng, J. Wen, D. J. Miller, Y. Meng, W. Yang, W. L. Mao, and H.-K. Mao, Synthesis of quenchable amorphous diamond, Nat. Commun. **8**, 322 (2017).

[38] Y. Lin, L. Zhang, H.-K. Mao, P. Chow, Y. Xiao, M. Baldini, J. Shu, and W. L. Mao, Amorphous Diamond: A High-Pressure Superhard Carbon Allotrope, Phys. Rev. Lett. **107**, 175504 (2011).

[39] L. Tan, H. Sheng, H. Lou, B. Cheng, Y. Xuan, V. B. Prakapenka, E. Greenberg, Q. Zeng, F. Peng, and Z. Zeng, High-Pressure tetrahedral amorphous carbon synthesized by compressing glassy carbon at room temperature, J. Phys. Chem. C **124**, 5489 (2020).

[40] N. A. Solopova, N. Dubrovinskaia, and L. Dubrovinsky, Raman spectroscopy of glassy carbon up to 60 GPa, Appl. Phys. Lett. **102**, 121909 (2013).

[41] Y. Shibazaki, Y. Kono, and G. Shen, Compressed glassy carbon maintaining graphite-like structure with linkage formation between graphene layers, Sci. Rep. **9**, 7531 (2019).

[42] P. Cataldi, A. Athanassiou, and I. S. Bayer, Graphene nanoplatelets-based advanced materials and recent progress in sustainable applications, Appl. Sci. **8**, 1438 (2018).

[43] S. Lu, M. Yao, X. Yang, Q. Li, J. Xiao, Z. Yao, L. Jiang, R. Liu, B. Liu, S. Chen, B. Zou, and T. Cui, High pressure transformation of graphene nanoplates: A Raman study, Chem. Phys. Lett. **585**, 101 (2013).

[44] A. F. Goncharov, Graphite at high pressures: Pseudomelting at 44 GPa, High Press. Res. **8**, 430 (1991).

[45] A. F. Goncharov, I. N. Makarenko, and S. M. Stishov, Graphite at pressures up to 55 GPa: Optical properties and Raman scattering-amorphous carbon? High Press. Res. **4**, 345 (1990).

[46] I. Efthimiopoulos, S. Mayanna, E. Stavrou, A. Torode, and Y. Wang, Extracting the anharmonic properties of the G-Band in graphene nanoplatelets, J. Phys. Chem. C **124**, 4835 (2020).

[47] C. Prescher and V. B. Prakapenka, DIOPTAS: A program for reduction of two-dimensional x-ray diffraction data and data exploration, High Press. Res. **35**, 223 (2015).

[48] B. H. Toby, EXPGUI, a graphical user interface for GSAS, J. Appl. Crystallogr. **34**, 210 (2001).

[49] K. Syassen, Ruby under pressure, High Press. Res. **28**, 75 (2008).

[50] A. Dewaele, F. Datchi, P. Loubeyre, and M. Mezouar, High pressure-high temperature equations of state of neon and diamond, Phys. Rev. B **77**, 094106 (2008).

[51] R. J. Hemley, C. S. Zha, A. P. Jephcoat, H. K. Mao, L. W. Finger, and D. E. Cox, X-ray diffraction and equation of state of solid neon to 110 GPa, Phys. Rev. B **39**, 11820 (1989).

[52] D. M. Ceperley and B. J. Alder, Ground State of the Electron Gas by a Stochastic Method, Phys. Rev. Lett. **45**, 566 (1980).

[53] J. P. Perdew and A. Zunger, Self-interaction correction to density-functional approximations for many-electron systems, Phys. Rev. B **23**, 5048 (1981).

[54] D. Vanderbilt, Soft self-consistent pseudopotentials in a generalized eigenvalue formalism, Phys. Rev. B **41**, 7892 (1990).

[55] R. M. Wentzcovitch, Invariant molecular-dynamics approach to structural phase transitions, Phys. Rev. B **44**, 2358 (1991).

[56] R. M. Wentzcovitch, J. L. Martins, and G. D. Price, *Ab Initio* Molecular Dynamics with Variable Cell Shape: Application to $MgSiO_3$, Phys. Rev. Lett. **70**, 3947 (1993).

[57] S. Baroni, S. de Gironcoli, A. D. Corso, and P. Giannozzi, Phonons and related crystal properties from density-functional perturbation theory, Rev. Mod. Phys. **73**, 515 (2001).

[58] P. Giannozzi, S. de Gironcoli, P. Pavone, and S. Baroni, *Ab initio* calculation of phonon dispersions in semiconductors, Phys. Rev. B **43**, 7231 (1991).

[59] See Supplemental Material at http://link.aps.org/supplemental/10.1103/PhysRevB.107.184102 for additional XRD, Raman, and DFT data.

[60] F. Occelli, P. Loubeyre, and R. Letoullec, Properties of diamond under hydrostaticpressures up to 140 GPa, Nat. Mater. **2**, 151 (2003).

[61] L. Pauling, The structure and properties of graphite and boron nitride, Proc. Natl. Acad. Sci. **56**, 1646 (1966).

[62] F. Birch, Finite strain isotherm and velocities for single-crystal and polycrystalline NaCl at high-pressures and 300-Degree-K, J. Geophys. Res. **83**, 1257 (1978).

[63] F. Birch, Finite elastic strain of cubic crystals, Phys. Rev. **71**, 809 (1947).

[64] J. A. Flores-Livas, L. Lehtovaara, M. Amsler, S. Goedecker, S. Pailhes, S. Botti, A. SanMiguel, and M. A. L. Marques, Raman activity of Sp^3 carbon allotropes under pressure: A density functional theory study, Phys. Rev. B **85**, 155428 (2012).

[65] C. S. G. Cousins, Elasticity of carbon allotropes. IV. rhombohedral graphite: Elasticity, zone-center optic modes,and phase transformation using transferred Keating parameters, Phys. Rev. B **67**, 024110 (2003).

[66] M. Mohr, J. Maultzsch, E. Dobardzic, S. Reich, I. Milosevic, M. Damnjanovic, A. Bosak, M. Krisch, and C. Thomsen, Phonon dispersion of graphite by inelastic x-ray scattering, Phys. Rev. B **76**, 035439 (2007).

[67] B. Li, Y. Nan, X. Zhao, X. Song, H. Li, J. Wu, and L. Su, Carbon nanohorns under cold compression to 40 GPa: Raman Scattering and x-ray diffraction experiments, Appl. Phys. Lett. **111**, 221905 (2017).

[68] A. F. Goncharov and V. D. Andreev, Raman scattering in carbon films at high pressure, Zh. Eksp. Teor. Fiz. **100**, 251 (1991) [Sov. Phys. JETP **73**, 140 (1991)].

[69] J. M. Montgomery, B. Kiefer, and K. K. M. Lee, Determining the high-pressure phase transition in highly-ordered pyrolitic graphite with time-dependent electrical resistance measurements, J. Appl. Phys. **110**, 043725 (2011).

[70] T. B. Shiell, C. de Tomas, D. G. McCulloch, D. R. McKenzie, A. Basu, I. Suarez-Martinez, N. A. Marks, R. Boehler, B. Haberl, and J. E. Bradby, *In situ* analysis of the structural transformation of glassy carbon under compression at room temperature, Phys. Rev. B **99**, 024114 (2019).

[71] T. B. Shiell, D. G. McCulloch, D. R. McKenzie, M. R. Field, B. Haberl, R. Boehler, B. A. Cook, C. de Tomas, I. Suarez-Martinez, N. A. Marks, and J. E. Bradby, Graphitization of Glassy Carbon After Compression at Room Temperature, Phys. Rev. Lett. **120**, 215701 (2018).

[72] S. Scandolo, M. Bernasconi, G. L. Chiarotti, P. Focher, and E. Tosatti, Pressure-Induced Transformation Path of Graphite to Diamond, Phys. Rev. Lett. **74**, 4015 (1995).

[73] R. Z. Khaliullin, H. Eshet, T. D. Kuhne, J. Behler, and M. Parrinello, Nucleation mechanism for the direct graphite-to-diamond phase transition, Nat. Mater. **10**, 693 (2011).

[74] S. Fahy, S. G. Louie, and M. L. Cohen, Pseudopotential total-energy study of the transition from rhombohedral graphite to diamond, Phys. Rev. B **34**, 1191 (1986).

[75] S. Fahy, S. G. Louie, and M. L. Cohen, Theoretical total-energy study of the transformation of graphite into hexagonal diamond, Phys. Rev. B **35**, 7623 (1987).

[76] X. Shi, C. He, C. J. Pickard, C. Tang, and J. Zhong, Stochastic generation of complex crystal structures combining group and graph theory with application to carbon, Phys. Rev. B **97**, 014104 (2018).

[77] H. Xie, F. Yin, T. Yu, J.-T. Wang, and C. Liang, Mechanism for direct graphite-to-diamond phase transition, Sci. Rep. **4**, 5930 (2014).

[78] Compared to the well-known 'AB' stacking sequence of HG, the RG and OG phases consist of 'ABC' and 'ABA' stacking orderings.

[79] H. Lipson and A. R. Stokes, The structure of graphite, Proc. R. Soc. A **181**, 101 (1942).

[80] E. J. Freise and A. Kelly, The deformation of graphite crystals and the production of the rhombohedral form, Philos. Mag. **8**, 1519 (1963).